Earthquakes and Structures, *Vol. 16, No. 4 (2019) 455-468*
DOI: https://doi.org/10.12989/eas.2019.16.4.455

Behavior of full-scale prestressed pile-deck connections for wharves under cyclic loading

Carlos A. Blandon[*1], Christopher J. Krier[2] and José I. Restrepo[3]

[1]*Department of Civil Engineering, EIA University, Km 2 +200 Variante Aeropuerto. JMC, Envigado, Colombia*
[2]*NV5, 2650 18th Street, Suite 202, Denver, Colorado 80211, USA*
[3]*Department of Civil Engineering, University of California San Diego, 9500 Gilman Dr, La Jolla, CA 92093, USA*

(Received April 20, 2018, Revised March 5, 2019, Accepted March 17, 2019)

Abstract. The behavior of pile-deck connections of pile-supported marginal wharfs subjected to earthquake loading is of key importance to ensure a good performance of this type of structures. Two precast-pretensioned pile-deck connections used in the construction of pile-supported marginal wharfs were tested under cyclic loading. The first is a connection with simple reinforcement details and light steel ratio developed for use where moderate pile-deck rotation demands are expected in the wharf. The second is specifically developed to sustain the large rotation, shear force and bending moment demands, as required for the shortest piles in a marginal wharf. Data obtained from the test program is used in the paper to calibrate an equivalent plastic hinge length that can be incorporated into nonlinear analysis models of these structures when prestressed pile-deck connections with duct embedded dowels are used.

Keywords: marine structures; performance-based seismic design; prestressed piles; pile-deck connection; seismic design; testing; wharves

1. Introduction

Due to the damaging effects of past earthquakes, design methodologies for port structures have moved towards performance-based (PIANC 2002). This trend has also been followed by port owners and code developers whom in recent years have issued design guidelines for seafront structures (POLA 2010; POLB 2012; Johnson *et al*.2013; ASCE, 2014). These codes establish performance levels for different earthquake intensities that are defined by specific concrete and steel strains at various locations of critical sections of the structure including the pile-deck connection.

This paper describes the seismic performance of two typical pile-deck connections employed in pile-supported container wharfs in Southern California which have been designed with specific details aimed to reduce construction times. In these structures the piles at and near the landside have relative short clear heights, whereas, the piles tend to be quite slender on the seaside. This geometrical characteristic means that during an earthquake the pile-deck connection at the landside will have significantly larger rotational demands than those at the seaside.

The test specimens were built at full-scale and then tested under quasi-static reversed cyclic loading at the University of California, San Diego. One of the specimens represented a pile-deck connection situated at the landside of the wharf where shear and rotation demands are the largest. The other specimen represented a connection located at a position closer to the seaside where the rotational and shear demands are not as large as those expected for the shorter landside piles.

The aim of the tests was to verify the overall performance of the connection and to obtain experimental data to validate the material strain limits that have been chosen in the development of the performance-based design code for marginal wharfs. The data from the tests was also used to estimate an equation for the plastic hinge length of prestressed pile-deck connections.

2. Background

2.1 Marginal wharf typology

A typical pile supported marginal container wharf, see Fig. 1, consists of a heavy duty deck supported on several rows of piles of different lengths which are driven inside the ground. The slope consists on quarry-run material with a top layer of rip rap to protect the slope from erosion

Apart from carrying the tributary deck self-weight and container loading, pile rows have specific functions. For example, piles on rows *B* and *G* in the wharf depicted in Fig. 1 support the load of the gantry crane while piles on rows *F* and *G* resist a large percentage of the earthquake, mooring and berthing lateral forces due to the low slenderness ratio. Under imposed lateral displacements at the deck level, the largest seismic rotation demands occur at the pile-deck connections in these two rows (Blandon 2013).

For large intensity earthquakes, these piles on rows *F* and *G* are expected to undergo large inelastic rotations while carrying significant shear. On the other hand, those

∗Corresponding author, Professor
E-mail: carlos.blandon@eia.edu.co

http://www.techno-press.com/journals/eas&subpage=7
ISSN: 2092-7614 (Print), 2092-7622 (Online)

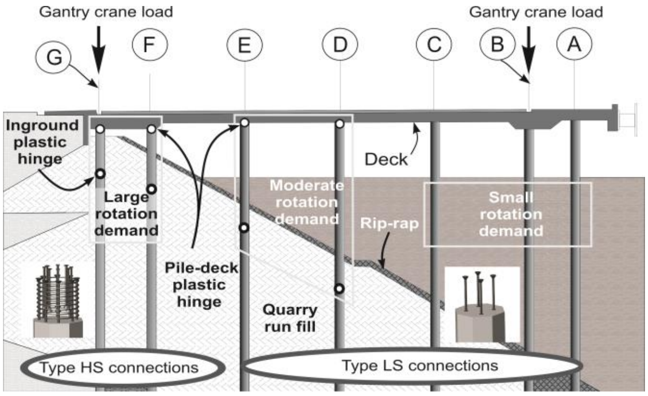

Fig. 1 Typical marginal pile supported wharf configuration

connections on rows *A* to *C* will most likely remain elastic and carry little shear. Those piles in rows *D* and *E* may experience some inelastic rotation demands while carrying significantly less shear than those piles on rows *F* and *G*. Plastic hinges are expected to occur at the pile-deck connection for the most demanded piles. Another plastic hinge is also expected below ground and an inflection point should appear between these hinges.

2.2 Connection types and design criteria

The different demand level justifies the use of two different types of pile-to-deck connection details: Type HS, for high-shear and Type LS, for low-shear. Type HS connections are detailed to carry high-shear and bending, to exhibit large nonlinear rotation capacity, and to display a stable hysteretic response. Type LS connections are required to exhibit moderate nonlinear rotation capacity while carrying a smaller shear force, compared to the HS connection. Type HS connections are suitable for the shorter landside piles in rows *F* and *G*, whereas Type LS connections are suitable for the more numerous longer seaside piles on rows *A* to *E*, see Fig. 1.

2.3 Research work on pile- deck connections

The use of double-headed dowel bars for pile-deck connections in wharves was introduced based on a full scale test on a cast-in-place concrete pile-cap connection reported Sritharan and Priestley (1998). The main objective of the test was to verify an innovative way to achieve a ductile moment-resisting connection that would ease constructability. The pile-deck connection was achieved with the use of single headed dowel bars. A dowel bar is a term used in these marine structures for the mild steel longitudinal reinforcement that protrudes from the pile end and is anchored in the deck. The main conclusion drawn from this test program was that the connection had a stable response and displayed rotation capacity exceeding 0.06 radians.

Tests of eight scaled pile-deck connections were reported by Roeder *et al.* (2002). Two test specimens incorporated cast-in place pile extension in the connections and six incorporated precast-pretensioned concrete piles and grouted dowel bars. Besides the type of pile, the main variable in this test program was the reinforcing detail at the pile-deck connection. The connection was achieved through the use of different dowel bar configurations and included dowel bars with hooks bent outward or inward, headed dowel bars and lap-spliced headed dowel bars. Some connections incorporated joint shear reinforcement and others did not. These researchers concluded that all connections tested are able to attain rotations at the pile-deck connection of up to 0.1 radians.

Blandon *et al.* (2011) reported the seismic response of two full-scale pile-deck connections of marginal wharves built in the 1980s at the POLA. One of the tests represented a precast pretensioned concrete pile-deck connection whereas the other represented a typical steel HP pile-deck connection. These tests were performed to assess the rotation capacity of existing connections under reversed cyclic loading. Moreover, the HP pile-deck connection was also proof-tested for the transient gantry crane wheel load. Both connections were able to carry the imposed axial load throughout, even when the flexural strength had degraded. The precast pile-deck connection maintained the flexural strength up to a rotation of 0.04 radians. The steel pile-deck connection maintained its flexural strength up to a rotation of 0.015 radians only.

Lehman *et al.* (2013) reported the test of eight full scale specimen where seven of them included details such as debonded dowels, interface bearing pads or isolation between the pile and the deck, aiming to improve the performance of the connection. Such modification showed to delay damage at the interface reaching larger drift with more limited damage. Wang *et al.* (2014) and Yang and Wang (2016) reported the test of six pile-deck high strength concrete connections with different details which included welded plates and inclined dowels at the pile top. The results from the tests indicate a poor cyclic behavior of these connections due to significantly pinched hysteretic loops and minimal energy dissipation. Larosche *et al.* (2013) reported the test of six pile-deck connection specimens where three of them aimed to evaluate the performance of plain embedded piles for exterior bent caps for bridges and wharves. The results from the tests show that the embedded piles developed a ductility capacity larger than 14% and were more economical to build.

In spite of the multiple options for pile-deck connections, the details proposed by Sritharan and Priestley (1998) are still widely used and the performance levels defined by current design guidelines, for precast concrete piles, have been developed considering this type of connections. Some of the tests reported by Roeder (2002) and Lehman (2013) consider these details; however, none of these specimens were tested considering the actual boundary conditions of the most demanded piles at the exterior bent, where the pile suffers a significant variation of the axial load, when subjected to lateral displacements, due to the coupling effect with the deck. Additionally, tests have been carried out for connections where large ductility demands are expected. Experimental information is required for pile-deck connections subjected to moderated or low ductility demands built with reduced steel detailing.

Regarding the numerical modeling of pile-deck

Table 1 Material strain for performance limit

Strain Limit	MD	CRD	LSP
Concrete compressive strain, ε_c	≤ 0.005	$\leq 0.005 + 1.1\ \rho_s$ ≤ 0.020	No limit
Grouted dowel tensile strain, ε_s	≤ 0.015	≤ 0.060 $\leq 0.6\varepsilon_{smd}$	≤ 0.080 $\leq 0.8\varepsilon_{smd}$

connections for wharves, several studies have been carried out with the scope of evaluating the response of wharf structures under lateral loading (Goel 2010,Shafieezadeh *et al.* 2012, Caiza-Sánchez *et al.* 2012, Chiaramonte *et al.* 2013, Doran *et al.* 2015, Yang and Wang 2016, Su *et al.* 2017). These studies have been mainly carried out using a fiber approach to model the section and using predefined plastic hinge lengths for the critical sections at the pile-deck connection. The estimation of this plastic hinge has been based on previous studies (Zhao and Sritharan 2007, Priestley *et al*. 1996). However, the plastic hinges defined by such references have been obtained from experimental data that does not match the specific details of the connections used for wharves. Precast piles usually have steel ducts where the dowels are grouted and prestressing strands are cut flush at the pile top. The deck may also have a large amount of transverse steel around the dowels. Such conditions may cause a significant effect on the plastic hinge length. Experimental data is required to define a plastic hinge length that could be used for modelling of pile-deck connections of wharves.

2.4 Performance levels and Structural strain limit-states

The structural performance of pile-deck connections is best defined according to the material strains at the pile-deck interface. For instance, ASCE/COPRI 61-14 standard (ASCE 2014) defines performance levels for three defined earthquake intensities: Operating Level Earthquake (OLE), Contingency Level Earthquake (CLE) and Design Level Earthquake (DE), defined as motions with a 50% of exceedance on 50 years, 10% of exceedance in 50 years and 2/3 of the Maximum Considered Earthquake as defined in ASCE-7 code (ASCE 2005), respectively. Each one of these intensities has an expected structural performance associated. For OLE, minimal damage to the structure is expected and minimum or no interruption of port operations may occur during repairs; for CLE a controlled level of inelasticity with minimum permanent deformation is expected and a short operations interruption may occur. Damage should be visible and accessible for repairs. Finally, DE is defined as life safeguard against major structural failure. Performance limits associated to these levels of intensity are minimal damage (MD), controlled and reparable damage (CRD) and life safety protection (LSP). Table 1 lists the material strains at the pile-deck connection for each performance level for solid concrete piles as stated by ASCE/COPRI 61-14 standard (ASCE, 2014).

3. Experimental work

Two full scale specimens were built following the actual practice used in the Port of Los Angeles which is aimed to reduce the construction time of the wharf. The specimens were tested under quasi-static reverse cyclic loading at the Charles Lee Powell Structures Laboratory of the University of California at San Diego. The first specimen tested investigated the performance of Type LS pile-deck connection, which is the connection with moderated rotation demands on the wharf, see row *E* in Fig 1. The second specimen tested investigated the performance of the HS pile-deck connection, which is the type of connection with the largest rotation demands on the wharf, see row *G* in Fig. 1.

To reduce the size of the full scale specimen only the pile-deck section above the inflection point located between the pile-deck hinge and the in-ground hinge of the pile was tested. However, the test set up was defined so the boundary conditions applied to the specimen would be representative of the conditions of the actual structure. The pile length between the connection interface and the inflection point was estimated based on a set of nonlinear pushover analyses which included the soil-structure interaction. The structural system including pile, deck and pile-deck interface was modeled with finite element nonlinear elements. The soil was modeled with nonlinear *p-y* springs defined based on properties used in common practice by geotechnical specialists for the quarry-run fill used for port construction at the Port of Los Angeles. For wharf design lower and upper bounds for the soil parameters are used depending on the type of demand that requires being estimated. i.e., shear, rotation or displacement. However, to estimate the location of the inflection line average soil parameters were used. These analyses revealed that inground plastic hinges will develop within the quarry-run fill, just below the rip-rap erosion control layer, see Fig. 1. An extensive report on the sensitivity analysis carried out using different modeling approaches and soil conditions may be found elsewhere (Blandon, 2007). The test specimens were capacity designed to ensure the development of plastic hinges at the pile-deck connection. These two specimens are described below in detail.

The pretensioned piles were built in a precast construction yard and transported to the site. After that, the piles were erected and aligned vertically and the dowel bars were grouted following the same standard procedure applied at the actual construction site

3.1 LS test specimen

Fig. 2 shows the main reinforcing details and dimensions of the LS test specimen. This test specimen is essentially a cutout around the pile row *E* from the top of the deck to the inflection point in the pile as shown in Fig. 1. The test specimen had a 0.61 m precast pretensioned octagonal pile with a length of 1.95 m from the soffit of the deck to the point of inflection, see Figs. 2(a)-2(c). The pile was built incorporating four 48 mm diameter by 2.0 m long corrugated steel ducts, and was prestressed with sixteen 15

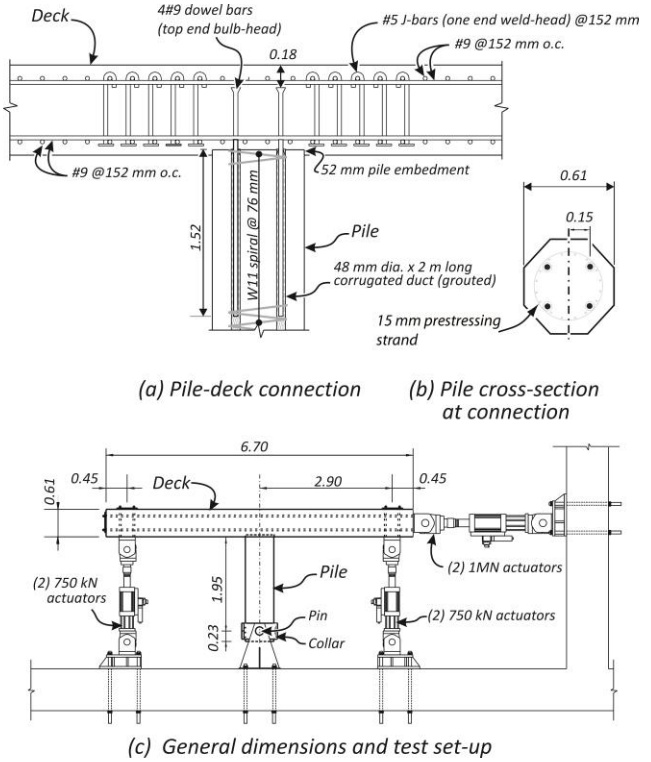

Fig. 2 LS specimen details and test set up

mm diameter low-relaxation strands. Four ASTM A706 #9 pile-deck dowel bars were grouted 1.52 m into the ducts. These bars had a bulb-head at their top for improved anchorage in the cast-in-place deck, see Fig. 2(a). The construction method employing grouted mild steel reinforcement has been used in the construction of emulative connections in buildings. The transverse reinforcement in the pile consisted of ASTM A82 W11 (A_{sh}=71 mm^2) spiral with 76 mm pitch. In order to enhance shear transfer, the pile was cut flush at both ends and erected in position to ensure 52 mm embedment into the concrete deck. The joint was expected to remain uncracked as the computed joint principal tensile stresses were 12% smaller than the concrete tensile strength (see Appendix 1). Consequently, the pile-deck joint was built without any joint shear reinforcement. The deck in the LS test specimen was 6.70 m long by 3.05 m wide by 0.61 m thick and was reinforced with top and bottom mats consisting of #9 bars spaced 152 mm in both directions. An array of punching shear reinforcement, consisting of #5 J-bars with a weld head at one end, was placed in the deck surrounding the pile. The pile was roughened at its base, erected and placed inside an oversized steel collar, see Fig. 2(c). The gap left between the pile and the collar was grouted. The pin holding the steel collar ensured a point of inflection at this location.

The test set-up for the LS test specimen is illustrated in Fig. 2(c). Lateral force was applied via two 1 MN capacity servo-controlled hydraulic actuators. These actuators were connected to the deck through sleeved rods that were fastened at the opposite end of the deck. Such connection detail implies that in the push and pull directions one side of the deck was subjected to compression by the horizontal

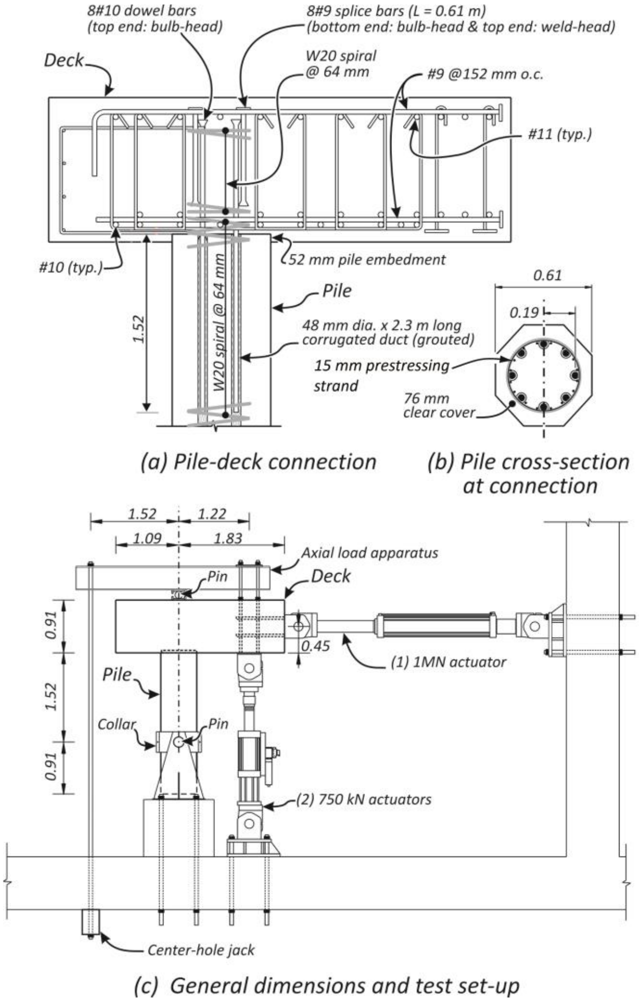

Fig. 3 HS specimen details and test set up

actuators. The deck vertical shear forces were resisted by two pairs of 750 kN capacity servo-controlled hydraulic actuators, with each pair located near the end of the deck, where the lines of inflection in the deck are estimated to occur in the prototype structure.

3.2 HS test specimen

Fig. 3 depicts the main reinforcement and general dimensions of the HS test specimen. Like in the LS test specimen, this specimen incorporated a 0.61 m octagonal precast pretensioned pile. The pile incorporated eight 48 mm diameter by 2.3 m long corrugated steel ducts, and was prestressed with sixteen 16 mm diameter strands, and had an ASTM A82 W20 (129 mm^2) spiral with 63 mm pitch, see Figs. 3(a)-3(b). The pile was cut to expose 1-1/2 turns of the smooth wire spiral to prevent unraveling of the spiral expected upon concrete spalling on the pile at the pile-deck connection and was cut to a specific length to ensure 52 mm of pile embedment within the deck. Eight ASTM A706 #10 bulb-head dowel bars were grouted in these ducts. For constructability, these bars ended below the deck top mat reinforcement. Joint principal tensile stress calculations indicate the joint in this connection was likely to crack (see Appendix 1). The joint principal tensile stress in this test was calculated as 138% the concrete tensile strength. Because of the likelihood of joint cracking and of a potential for joint shear strength degradation, each #10 dowel bar was lap-spliced with a ASTM A706 #9 bulb-headed bars that were anchored above the top mat of reinforcement, enabling the development of a truss mechanism of internal force transfer. Twelve turns of ASTM A82 W20 (A_b=129 mm^2) with a 63.5 mm pitch were provided as joint reinforcing to transfer joint shear and to also enhance the splice conditions between the grouted bars and the bulb-end headed bars. The deck in the HS test specimen was 2.92 m long by 1.52 m wide by 0.91 m thick. The deck was reinforced with a top mat consisting of #9 and #11 bars, a bottom mat consisting of #9 and #10 bars, plus shear and trim reinforcement. The larger top and bottom diameter bars, and the shear reinforcement were provided in the deck of the prototype structure to resist flexure caused by the gantry crane. The distance between the deck soffit and the pin holding the steel collar was 1.52 m, see Fig. 3(c). The pile was grouted to the collar near its base. Because large axial forces were expected to develop in the pile in this test specimen, the pile was extended 0.91 m below the mid-height of the collar to provide sufficient development length for the strands.

Cyclic lateral forces were applied through a single 1 MN capacity servo-controlled hydraulic actuator; see Fig. 3(c). This actuator was connected through rods cast-in with the concrete. This implies that the deck right hand portion was subjected by the actuator to axial tension and compression. Additionally, a pair of 750 kN capacity servo-controlled hydraulic actuators where placed in parallel to the column at the right hand side, with the specific task of restraining the deck rotation but allowing the vertical displacement. The left hand side of the deck was left to cantilever from the pile, as is the case in pile rows *G* shown in Fig. 1. The boundary conditions were aimed at representing the actual conditions of the structure, which, under lateral loading cycles, induce a variable axial load on the pile, in addition to shear and bending.

(a) Pile of LS test specimen (b) Pile top of HS test specimen

Fig. 4 Specimens during construction

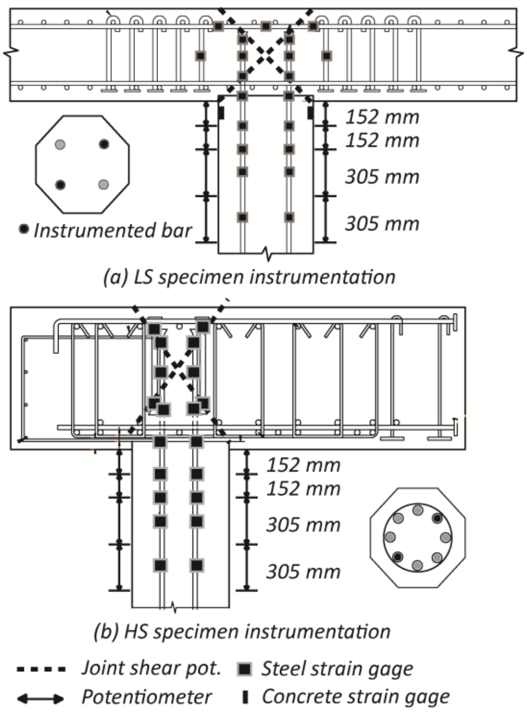

(a) LS specimen instrumentation

(b) HS specimen instrumentation

Fig. 5 Instrumentation layout

4. Material properties

The grout used for the dowels consisted of water (w) and ordinary Portland cement (c) mixed to a w/c ratio of 0.4 per weight. A commercial superplasticizer was added to the admixture at a dose of about 250 ml per 356 N (80 lbs) of cement. Formwork was prepared for the deck, which was cast in the upright position in both test specimens. Fig. 4 shows the piles of test specimens during construction.

The concrete compressive strength obtained for the LS test specimen at the day of the test was 49.5 MPa for the deck (at 37 days of age) and 41.4 MPa for the duct grout (at 42 days). The pile concrete strength at 28 days was 57.2 MPa. For the HS specimen, the concrete strength was 37.2 MPa for the deck (at 38 days) and 40.0 MPa for the duct grout (14 days). The pile concrete strength at 28 days was 55.8 MPa. For both specimens, the #9 dowel and splice bars had a yield strength of 469 MPa, an ultimate tensile strength of 641 MPa and a tensile strain at peak tensile force of 16.0%. The #10 dowel bars had yield strength of 476 MPa, an ultimate tensile strength of 669 MPa and a tensile strain at peak tensile force of 11.2%.

5. Test setup and instrumentation

The test specimens were extensively instrumented based on previous experience to obtain key information about the pile-deck connection, dowel bar strain distribution and joint deformations (Restrepo *et al*. 1995). The instrumentation was concentrated around the pile-deck connection, where plasticity was expected to occur. Rotations were measured along the pile length by four pairs of displacement transducers located on either side of the pile at 152 mm, 304 mm, 610 mm and 914 mm from the bottom of the deck. Four string potentiometers were deployed in x-shape through the joint core in four 12 mm (1/2 in.) diameter PVC tubes that ran through the deck on either side of the pile. These sensors were placed for measuring joint shear distortions during loading. Additionally, several strain gages

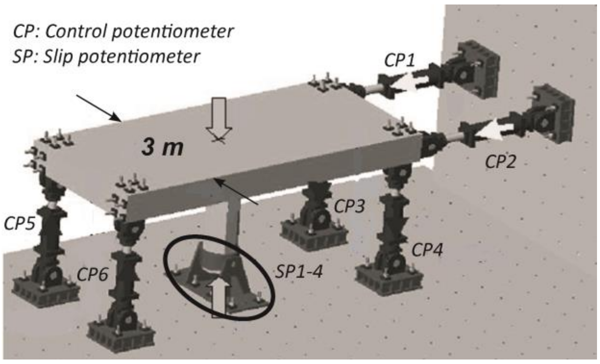

(a) LS test control setup

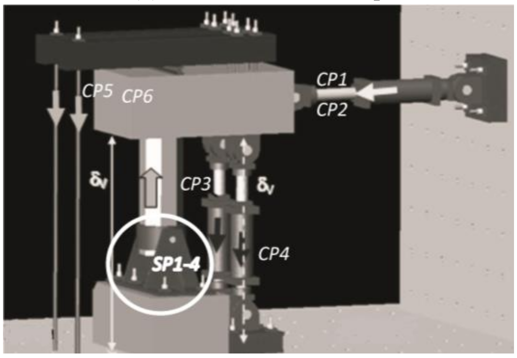

(b) HS control setup

Fig. 6 Sensors for test control

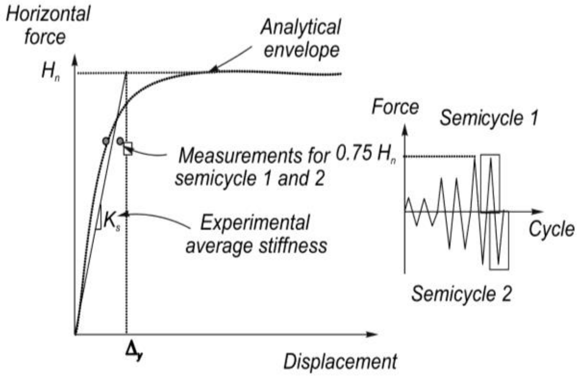

Fig. 7 Yield displacement definition

were placed along connection bars to evaluate the yield spreading (see Fig. 5).

Vertical string potentiometers were placed at several locations between the base of the reaction floor and the bottom of the deck for test control purposes. Horizontal and vertical displacements were measured with string potentiometers. Displacement transducers were placed between the pile and the steel collar used to fix the column at the base. Additional sensors were also placed between the floor and the collar and between the pile and the floor. These sensors were aimed at monitoring possible rigid body displacements. 5 mm long electrical foil strains gages were installed along two opposite dowels at the connection every 152 mm, extending 458 mm inside the deck and 762 mm inside the pile.

Fig. 6 depicts a rendering of the test specimens and the key sensors location used for control. CP1 and CP2 are the horizontal control potentiometers and CP3 to CP5 are the vertical control potentiometers. SP1 to SP4 are potentiometers located at the pile-collar connection. Control algorithms were written to actively control the vertical actuators to ensure the deck remained horizontal throughout testing, and to ensure it could move vertically because of the possible axial elongation or shortening of the pile at the pile-deck connection. For the particular case of the LS test specimen the control was also programmed to ensure the axial load in the pile remained constant and equal to the vertical load prior testing. This was achieved by incorporating the differences between the vertical displacement transducers measuring the displacement, δ_v, at either side of the pile into the vertical actuator feedback control loop. To avoid actuator command errors at large lateral displacements, all control algorithms accounted for geometrical nonlinearities of the deformed test specimens and of the actuators.

Testing was divided in two phases. The first phase was force-controlled whereas the second was displacement-controlled. The lateral force-controlled phase consisted of two complete cycles at each of four target lateral forces, namely 0.125, 0.25, 0.50, and 0.75 of the theoretical lateral force capacity, H_n. This capacity was calculated as the reference yield moment divided by the distance between the deck's soffit and the pile's point of inflection. The reference yield moment was calculated from a moment-curvature analysis of the pile section at the pile-deck interface, that is, the section with the steel dowel bars but not the prestressing strands, and determined as the moment at which the extreme bar in tension reached 1.5% strain or the extreme fiber in compression reached 0.4%, whichever occurred first (Priestley *et al*. 1996). This moment was readily calculated for the pile-deck connection on the LS test specimen but, because of the variation of axial force in the pile induced by the lateral displacement, the yield moment in the pile-deck connection of the HS test specimen was calculated through an iterative procedure that consisted on matching the correct combination of lateral load, axial load and pile-deck connection moment capacity. Second order effects were also considered for these analyses.

The displacement-controlled phase was based on displacement ductility increments of Δ_μ= 1, 1.5, 2, 3, 4, 6 and 8. Three complete cycles were prescribed for each ductility level. The displacement ductility was defined as $\mu_\Delta=\Delta/\Delta_y$, where was the applied lateral displacement and Δ_y was the reference yield displacement computed experimentally for the test specimen. Two parameters were employed to define Δ_y: the theoretical lateral force capacity, H_n, and the experimental lateral stiffness, K_s. The lateral stiffness was determined as the average of that obtained from the displacements measured at the two force-controlled semi-cycles corresponding to 0.75 H_n. Fig. 7 shows the procedure employed to define Δ_y.

At the beginning of testing, the pile of the LS test specimen carried an axial compressive force equal to the entire gravity load of the deck of P=293 kN whereas the pile of the HS test carried an axial compressive force of 67 kN. In addition to supporting lateral load and deformation during testing, pile rows supporting the crane wheel load should be able to resist this vertical force after an earthquake. To reproduce this condition, the axial force in the HS test specimen, representing row *G* in Fig. 1, was increased by P=455 kN during the entire third cycle at each prescribed ductility level in the displacement-controlled phase of the test. The additional axial force was applied on the deck directly above the pile via a pin supporting the axial load apparatus depicted in Fig. 3(c). The axial load on the HS test specimen was actively controlled and maintained constant during these cycles.

6. Test results

6.1 LS test specimen

According to ASCE/COPRI 61-14, the Minimum Damage performance level occurs when 1.5% tensile strain in the grouted dowel bars or 0.5% compressive strain in the pile concrete cover is reached. In this test specimen, the MD was governed by the grouted dowel bars when the 1.5% tensile strain was measured in the one of the extreme bars in tension at a connection rotation θ=0.0078 radians, which corresponds to a drift ratio Θ_r=0.90%, and a displacement ductility μ_Δ=1.5, see Fig. 8 (a) where the MD are marked on the lateral force-lateral displacement hysteretic response. The rotation was estimated based on the measurements of the displacement transducers located at opposite sides of the pile under the deck covering a 152 mm distance from the soffit. The drift ratio is defined here as the ratio between the deck lateral displacement (Δ) and the distance of 2.0 m between the pin at the base of the pile and pile end embedded 52 mm into the deck (*H*). The reference yield displacement, Δ_y, which defined μ_Δ=1, was reached at a drift ratio Θ_r=0.58%. Due to the large deck stiffness most of the contribution to the drift was due to the concentrated rotation at the pile-deck interface and in a second instance due to the pile flexibility.

In the pull direction, the dowel tensile strain limit of 1.5% occurred at a connection rotation θ=0.008 radians, which corresponds to a drift ratio Θ_r=0.10% (i.e., μ_Δ=1.7). Onset of spalling of the deck concrete cover around the pile was observed for this performance level. This damage occurred because of prying action of the pile in the deck concrete cover. This suggests that the MD may be caused by structural damage in parts of the wharf other than the piles.

Flaking of the pile concrete cover at the pile-deck connection occurred during the first cycle at a drift ratio Θ_r=3.4% (i.e., μ_Δ=5.8) corresponding to a pile-deck rotation of 0.032 radians. Limited spalling of the concrete cover occurred thereafter, which gives an indication that the neutral axis depth was indeed very shallow, as it had been calculated analytically. The CRD, which is established by ASCE 61-14 as that corresponding to a tensile strain of 6.0% in a dowel bar or a maximum compressive strain of 1.41% in the concrete (see Table 1), whichever is reached first, could not be measured directly as none of the strain gages placed on the dowel bars at the pile deck interface provided reliable data past a tensile strain ε_s=3.5%. However, given the shallow neutral axis depth and the damage pattern observed at the damaged section, it was inferred that CRD was governed by the tensile strain limit in the extreme dowel bar in tension, rather than by the strain limit in the concrete. Based on the extrapolation of the strains and corresponding rotations measured before and after the failure of the gages, the authors estimate the CRD was reached at an approximate lateral displacement of Δ=100 mm, when the connection attained a rotation θ=0.047 radians, and a drift ratio Θ=4.9 % (i.e., μ_Δ=8.4). Damage at this stage was limited to spalling of the bottom deck concrete and pile concrete at the interface with the deck. Reinforcement was not observed at this stage.

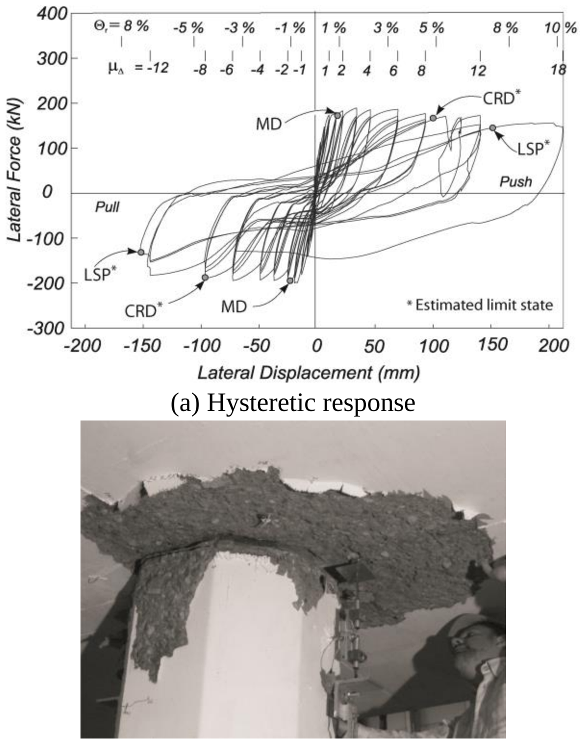

(a) Hysteretic response

(b) View of connection at the end of test

Fig. 8 Hysteretic response and damage at end of test for LS unit

By applying the same procedure, LSP was estimated to have occurred approximately for a lateral displacement of 152 mm at a drift ratio close to Θ =7.0% and a rotation θ=0.064 radians (i.e., μ_Δ=12). The lateral force at this instant was 92% of the peak force measured during the test.

A final cycle was applied to the structure after reaching the displacement ductility of 12. Fracture of reinforcement bars was obtained after unloading from the maximum displacement applied for this cycle, which exceeded 200 mm in the push direction and a drift ratio larger than 10%.

The lateral force-displacement hysteretic response for the LS test specimen, plotted in Fig. 8(a), provides evidence that the LS test specimen has a ductile behavior and, even if pinching of the response becomes more accentuated after Θ_r=1.0%, the hysteretic response is stable as second and third cycles to the same lateral displacement are quite similar for most part of the test.

Data reduction indicated that in the LS test specimen nearly all inelastic deformations concentrated at the pile-deck connection and insignificant spread of plasticity occurred along the length of the pile. The concentration of the rotation at the pile-deck interface was due to the presence of the strands in the prestressed pile, which limited the spread of plasticity along the pile. This is evident in Fig. 8(b) that shows the connection at the end of testing. In this test specimen there were not visible cracks at the joint but the pile and the deck showed slight cracking.

6.2 HS test specimen

In the HS test specimen, like in the previous test specimen, the MD was governed by the grouted dowel bars. In the push cycles when the pile was further compressed, the ε_s=1.5% tensile strain for the push cycles occurred at a connection rotation θ=0.029 radians, which corresponds to a drift ratio Θ_r=3.1%, and a displacement ductility μ_Δ=3.8. In this test specimen drift ratio is defined as the lateral displacement divided by 1.57 m, which is the distance between top of the pile where it was embedded 52 mm into the deck and the pin holding the steel collar near the bottom of the pile. The reference yield displacement, Δ_y, was reached at a drift ratio Θ_r=0.8%. For the pull cycles, when the pile became subjected to tension, the 1.5% tensile strain occurred at a connection rotation θ=0.015 radians, which corresponds to a drift ratio Θ_r=1.5%, and a displacement ductility μ_Δ=1.87. Rotations and drifts at MD were larger for push than for pull cycles. This is to be expected because during the pull cycles, when the pile is in tension, the neutral axis depth is shallower than in the push cycles, when the pile is being compressed. This also means that to reach a defined tensile limit strain in the extreme bars, a smaller rotation is required when the pile is in tension than when the pile is in compression.

Onset of spalling at the deck cover concrete was observed during the cycle with a maximum rotation of 0.012 radians. In the LS test specimen, detaching of the concrete cover was caused by prying action of the pile embedded within the deck. In this test specimen, the CRD could not be detected from direct measurements because of failure of the strain gages. According to the measured shallow neutral axis depth, it was also inferred that CRD was governed by the dowel tensile strain limit of ε_s=6.0%. From the rotation vs plastic strain plots in the critical dowel bar in tension it was estimated that the CRD was reached at a displacement of approximately Δ=106 mm in the pull direction when the pile was in tension. At this lateral displacement the pile-deck connection rotation was θ=0.065 radians, and the drift ratio and displacement ductility were Θ_r=6.7% and μ_Δ=8.4, respectively. Damage at this performance level was limted to the pile deck interface with spalling of the bottom deck concrete and at the pile interface. The damage was limited to the cover concrete and the steel was not compromised.

LSP was inferred to have occurred during the pull cycle for a lateral displacement of 138 mm approximately, which corresponded to a drift ratio and displacement ductility of Θ_r=9.0% and μ_Δ=11.2, respectively.

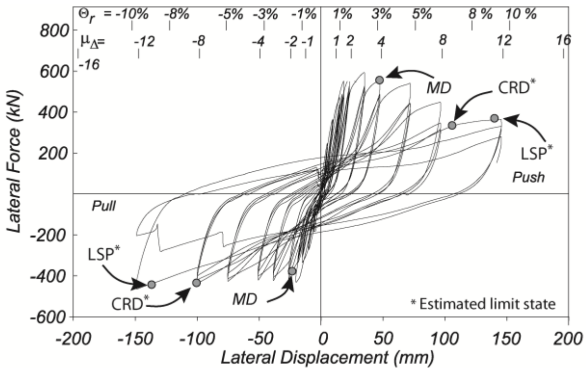

(a) Hysteretic response

(b) View of connection at the end of test

Fig. 9 Hysteretic response and damage at end of test for HS unit

The HS test specimen had an overall response with a displacement ductility capacity exceeding μ_Δ=10.0 before failure and good stability in the hysteretic loops in spite the second order effects during the pile compressive cycles, see Fig. 9(a). This test specimen was cycled to Δ=±152 mm, which corresponds to a connection rotation θ=0.096 radians, and a drift ratio Θ_r=9.7% (i.e., μ_Δ=12.1). Very little lateral strength degradation occurred for the push cycles up to Θ_r=4.8% (i.e., μ_Δ=6), when the rotation in the pile-deck connection was θ=0.044 radians. The loss of strength was mainly caused by the P-Delta effect. A pronounced loss of lateral strength occurred for the push cycles past Θ_r=4.8%. This was caused by spalling of the thick pile concrete cover immediately below the pile-deck connection, which reduced the pile moment capacity there. For the pull cycles, when the pile was in tension, significant strength and stiffness degradation was observed only during the second cycle to μ_Δ=12.1. Such degradation was caused by the fracture of some dowel bars. The presence of the crane wheel load, which was applied during the third cycle of each cycle, caused no damage to the pile or the connection. For all cycles where this load was applied, the pile maintained its vertical load carrying capacity.

In the HS test specimen inelastic deformations concentrated at the pile-deck connection and at the pile immediately below the pile-deck interface. There was limited spread of plasticity along the dowel bars and along the concrete at the pile top. The latter was manifested by spalling of the concrete cover during the push cycles, see Fig. 9(b) which shows the HS test specimen at the end of testing. Spalling of the concrete cover resulted in debonding of the strands in this region, which facilitated the spread of plasticity along the dowel bars into the pile. The x-shaped string potentiometers deployed in the joint region showed sudden peaks on the measurements which indicates that cracking occurred in the joint; however it was limited and joint shear deformations were only a minor contributor toward the lateral displacements imposed. There was an increase of the axial load in the push cycles and a decrease of compression forces and even tension in the pull cycles. Peak pile compressive and tensile axial forces, recorded in either the first and second cycles to a prescribed displacement, that is, of the cycles that did not include the additional crane load, were 977 kN (compressive) and 682 kN (tensile), respectively.

7. Discussion

The two tests discussed in this paper provide clear evidence that plasticity concentrates at the pile-deck connection. Tests by others (Roeder *et al*. 2001, Blandon *et al*. 2011, Blandon *et al.* 2013) also indicate that this is the case when precast pretensioned piles are used, and capacity design is applied to ensure that a plastic hinge develops at the connection. Furthermore, the piles are generally subjected to low axial loads and the variation of the axial load during seismic excitation, although it can be large in relation to the static load, still results in small net axial load level in these piles.

The observed behavior suggests that a lumped plasticity model (Giberson 1967) is an ideal candidate for modeling these connections for use in nonlinear structural analyses. A more sophisticated fiber model can also be used. The latter model has the advantage of considering the effects of the axial load variation on the flexural behavior of the pile-deck connection. The main purpose of either model is to relate the deformations of the structure induced by seismic actions to material damage strain limits at some critical locations including the pile-deck connections. This is a key objective in performance-based seismic design in the codes issued by the port authorities.

Both models make use of an equivalent plastic hinge length L_p to define the portion of the elements where the inelastic response occurs. The estimation of such parameter may significantly affect the results from the numerical models. According to the work by Mander *et al.* (1984) and Priestley and Park (1987) there are several main factors that have to be considered in the estimation of the plastic hinge which are the spread of plasticity along the element as result of the moment gradient, the steel reinforcement hardening, the inclined flexural-shear cracks and the strain penetration along the reinforcement bars into the adjacent elastic members. A well-known expression for regular reinforced concrete members was proposed by Paulay and Priestley (1992). L_p is the largest value obtained from the two expressions

$$L_p = 0.08H + 0.022 d_b f_y \tag{1a}$$

$$L_p = 0.044 d_b f_y \tag{1b}$$

H is the element length from the location of maximum moment to the point of inflection, d_b is the steel reinforcement bar diameter and f_y is the yield strength of the reinforcement. In Eq. (1a) the first term considers the spread of plasticity along the pile caused by a combination of moment variation and steel reinforcement hardening and the second term captures the strain penetration of the dowel bars that yield and damage the bond between the bar and the concrete, causing bond-slip within the deck and within the pretensioned pile. Eq. (1b) considers the case when the spread of plasticity due to the moment variation and steel hardening is limited and the main source of inelasticity is due to the strain penetration inside the element and inside the adjacent elastic member.

Based on the observed behavior during the test described previously as well as other tests (Blandon *et al*. 2011, Kawamata *et al*. 2007), the main source of inelasticity at the pile-deck connection is due to the strain penetration mechanisms. The spread of plasticity along the element is negligible as the cracks formed in the pile have are scarce and significantly narrow compared with the opening observed at the pile-deck interface. In the case of pretensioned piles, dowel bar plastic strains penetrate into the grouted ducts, causing bond damage and bond slip. This phenomenon does not occur along the length of a regular reinforced concrete element because the spread of plasticity along on such elements is a function of the tensile stress in the reinforcement, the amount of longitudinal reinforcement and is either a function of the bending moment gradient and/or of the shear reinforcement provided in the length of the column where the plastic hinge has developed (Hines *et al*. 2004).

Based on the observed behavior during the tests and the difference on the mechanics between prestressed elements and regular reinforced concrete elements, Eq. (1a) is disregarded for pile-deck connections of prestressed piles and an alternative form of Eq. (1b), is proposed.

$$L_p = k \frac{f_y}{E_s} d_b \tag{2}$$

This equation was defined as a function of the longitudinal bar diameter (d_b), the yield strength (f_y), the steel modulus of elasticity (E_s) and an empirically calibrated coefficient k. This coefficient can be approximately calculated, for the equation postulated by Paulay and Priestley (1992), as k=8900 when considering Eq. (1b).

Data obtained from seven different test specimens, including the LS and HS units, four units tested by Kawamata *et al*. (2007) and one more reported by Blandon *et al*. (2011), were used to carry out a regression analysis to obtain the value of k for the specific case of prestressed concrete pile-deck connections.

The analyses consisted on back-calculating the equivalent plastic hinge length using the experimental moment rotation envelopes from these seven specimens and numerical moment curvature envelopes for the same tests. Several values of k were obtained for each specimen, estimating the equivalent plastic hinge length that would match specific steel strains along the experimental moment rotation envelope with the corresponding steel strains from the numerical moment curvature envelope.

In all the experiments, the piles, the deck, the concrete, the grout, the anchorage details and the steel diameter had

Table 2 Material strain for Structural limit states

Parameter	Current study		Blandon *et al*. (2011)		Kawamata *et al*. (2007)						
Specimen and direction of loading	LS Push	HS Push	A1 Push	A1 Pull	P2 Push	P2 Pull	P4 Push	P4 Pull	P3 Push	P3 Pull	P5 Push
f_y (MPa)	469	469	466	466	466	466	466	466	466	466	466
f'_{cdeck} (MPa)	48.3	35	36.9	36.9	35.2	35.2	35.2	35.2	35.2	35.2	35.2
f'_{cgrout} (MPa)	47.0	47.0	47.0	47.0	-	-	-	-	-	-	-
f'_{cpile} (MPa)	57.2	55.8	52.8	52.8	56	56	56	56	56	56	56
d_b (mm)	29	32	29	29	32	32	32	32	32	32	32
ρ_l(%)	0.8	2.1	1.7	1.7	2.1	2.1	2.1	2.1	2.1	2.1	2.1
$\theta\varepsilon_{s1\%}$(milirad)	7.0	9.1	5.5	5.6	5.0	4.8	10.0	5.0	7.8	7.6	7.0
ε_{smax}(%)	3.5	1.65	4.3	4.7	2.0	3.0	2.0	1.1	3.0	2.0	3.3
$\theta\varepsilon_{smax}$(milirad)	31.3	15.8	25.6	20.0	11.0	15.0	18.0	8.0	21.0	12.0	20.0
K	3732	4800	2628	2208	2549	2549	3677	3541	4391	3258	3399

very similar characteristics and all the specimens were tested under relatively similar boundary conditions and load protocols. Damage and failure modes at the connection were also similar.

Data for the regression analysis comprised the range of strain and pile-deck rotations beginning from 1% tensile strain, measured in all tests, up to the maximum tensile strain measured during the tests when the strain gages were rendered unusable. Such strains and rotations, as well as the dowel bar yield strengths are listed in Table 2 for all specimens.

The regression analysis aimed at minimizing the error between measured strains and strains calculated from theoretical moment-rotation analysis, where the theoretical rotation was computed as the theoretical curvature times L_p, gave a mean value of k=3340 and a sample standard deviation of 812, which is high. Possible causes for such variation were evaluated including clear height, lateral shear force, moment gradient and axial load variation. However, the results obtained for k do not show a clear trend. Despite of the large dispersion it is clear that the plastic hinge length obtained for all the tests is considerably smaller than the value estimated by Eq. (1b).

Fig. 10 compares the theoretical and measured moment-rotation responses calculated for the LS and HS test specimens. The theoretical rotation was calculated as the curvature times L_p, using mean value of coefficient k. This approximation is considered to be sufficiently accurate as the elastic component of the rotation is negligible at the levels of strain used for the regression analysis. The markers on the envelopes show some experimentally measured strains and the corresponding numerically calculated strains using the k value proposed. The authors note that despite there is good agreement between the measured and calculated moment-rotation relationships, there is only a fair agreement between measured and calculated tensile strains.

Numerical models often consider the pile-deck connection using moment rotation relationships of a zero length spring element. These relationships are obtained from moment curvature of section analyses of the pile-deck interface. The rotation is then obtained by integrating the curvature along the equivalent plastic hinge length. When this procedure is used, the proposed equation for such length may be used for precast pile-deck connections with similar characteristics to those presented in this study as the resulting moment rotation relationship will consider a reduced plastic hinge length. Using equivalent plastic hinge lengths obtained for regular reinforced concrete may result in more flexible connections and non-realistic lower strain demands for the steel. Note that even for the average proposed value of k, which is around 37% of the most conservative value proposed by Paulay and Priestley (1992), the experimental measured strains in the steel were lower than the calculated strain values for the LS connection. For the HS connection, there was a good agreement for the pull cycles and only for the push cycles, the measured strains were larger than the calculated. Even if

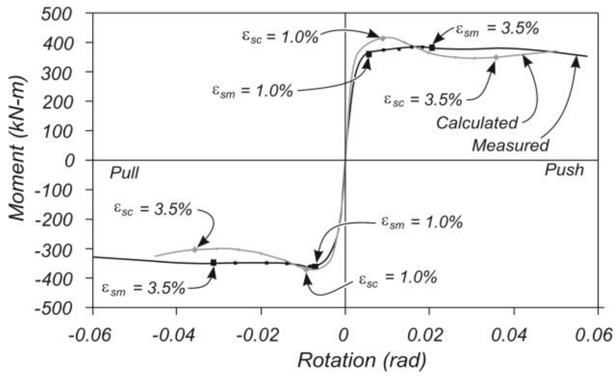

(a) LS test specimen

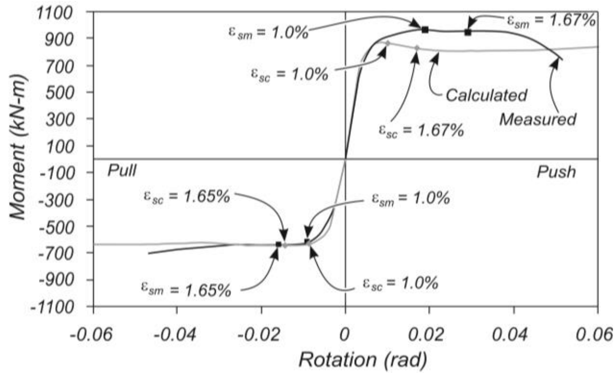

(b) HS test specimen

Fig. 10 Measured and calculated moment rotation response for LS and HS connections

Table 3 Pile-deck rotation at onset of spalling

Reference	Test unit	Pile-deck rotation at onset of spalling (milirad)
This work	LS	7
	HS	12
(Kawamata *et al*. 2007)	P2	7
	P4	10
	P3	14
	P5	6.5
(Blandon *et al*. 2011)	A1	15

there is a considerable dispersion in the data, the trend seems to indicate that is likely that a much shorter plastic hinge length should be used for the connections with duct embedded dowels than for cast in place concrete connections.

Results of the tests indicate that at the pile-deck interface there is a prying effect in which the embedded portion of the pile produces spalling of the deck concrete cover. This form of damage is not currently considered as a limit state in any of the existing codes or design guidelines. However, as the deck reinforcement may become exposed and corroded after the cover spalling a pile-deck rotation of 0.01 radians is proposed as an additional MD limit for this type of connection. Table 3 includes the pile-deck rotations values at which onset of spalling was observed. Additional values from Kawamata *et al*. (2007) and Blandon *et al*. (2011) are also included in the same table.

8. Conclusions

This paper presented the results of two precast pretensioned pile-deck test specimens of pile-supported marginal wharves. The connections in these test specimens were built at full-scale using construction practices established in pile-supported container wharfs in Southern California. The tests were conducted to support performance-based seismic codes currently used for marginal wharfs design. In these tests, the pile-deck connection was established using bulb-headed dowels grouted into corrugated ducts incorporated into the pile. One test specimen incorporated a pile-deck connection designed to resist high-shear and bending, to exhibit significant ductility capacity, and to display a stable hysteretic response (Type HS connection). The other connection was designed to resist low-shear and bending (Type LS connection). The research program had two main objectives: (i) to report the overall response and the development of various material damage limit-states in two specific pile-deck connections; and (ii) to calibrate an equivalent plastic hinge length for these connections for use in the nonlinear analysis of pile-supported marginal wharf structures.

The main conclusions drawn from this experimental program are:

1. Both connection types reached a rotation of at least 0.04 radians before any significant moment strength degradation occurred. The presence of strands in the prestressed piles hampered the spread of plasticity along the pile, which is opposed to the way it does in a conventional reinforced concrete member. Plasticity in these connections stemmed from bond slip of the bars that yielded into the deck and into the pile.
2. Gravity load results in relatively low axial load ratios in the piles in pile-supported marginal wharves. For this reason, extreme landside piles can experience axial load reversals that subject them to tension. For this axial load levels, the associated performance levels for the Operating and Contingency ground motions are controlled by the tensile strain in the extreme dowel bars in tension, rather than by the limiting strain of the concrete in compression. Such was the behavior observed in the tests. The Minimum Damage Level was defined at the point when the tensile strain in critical dowel bar measured 1.5%. In the specimen incorporating the Type LS connection, this strain was attained at a pile-deck connection rotation of 0.0078 radians. In the test specimen incorporating the HS connection, the 1.5% tensile strain limit-state was reached at a pile-deck connection rotation of 0.015 radians, when the test specimen was being pulled and the pile was in tension. Strain gages on the dowel bars failed before the 6.0% tensile strain limit. This strain limit marked the Controlled and Reparable Damage performance Level in the piles of the test units. Extrapolation of the plastic strains recorded prior to strain gage failure versus pile-deck rotation indicates that the 6.0% tensile strain should have been reached at a pile-deck connection equal to 0.047 and 0.065 radians in the low-shear and high-shear test specimens, respectively. As in the MD Level, the CRD Performance Level in the high-shear test specimen most likely occurred when the pile was in tension. The LSP limits were estimated to have occurred at drifts lower than the failure drifts for both specimen.
3. In both test specimens, the 52 mm of the pile embedment into the deck, pried the concrete cover of the deck and caused it to spall. A review of existing data indicates that this MD Level occurs at a pile-deck rotation of about 0.01 radians.
4. Pile-cap rotation and tensile strain data from the two specimens presented in this study and five more specimens on connections incorporating precast pretensioned piles with grouted dowels, reported in other references, was analyzed and used to calibrate a simple equivalent plastic hinge length equation for these type of connections. Statistical analysis of the data shows important variability but indicates a plastic hinge significantly smaller than those proposed in the existing literature. Such reduced plastic hinge length may be used in numerical models to prevent non-realistic connection stiffness and material strains.

Acknowledgements

The research program described in this paper was sponsored by the Port of Los Angeles. The full scale tests presented in this paper were performed at the Charles Lee Powell Laboratory of the University of California, San Diego. Dr. Chris Latham, Charlie Stearns, John Ward, Bob Parks, Ben Terrace, Andy Gunthardt, and Paul Greco deserve special recognition for their contribution in the construction and testing of the test specimens. This research program was made possible by the guidance and expertise provided by Peter Yin of the Port of Los Angeles, Professor Emeritus Nigel Priestley, Dr. Omar Jaradat, and Max Weismair and the assistance of Jared Bell. Additional funding for data post-processing was provided by the EIA University.

References

American Society of Civil Engineers (ASCE) (2005), Minimum Design Loads for Buildings and Other Structures, ASCE 7-05, American Society of Civil Engineers, Reston, VA.

ASCE/COPRI Committee 61 (2014), Seismic Design of Piers and Wharves, ASCE/COPRI 61-14, American Society of Civil Engineers

Blandon, C.A. (2007), "Seismic analysis and design of pile supported wharves", Ph.D. Dissertation, Centre for Post-Graduate Training and Research in Earthquake Engineering and Engineering Seismology (ROSE School), University of Pavia, Pavia, Italy.

Blandon, C.A., Bell, J., Restrepo, J.I., Jaradat, O., Yin, P. and Weismair, M. (2011), "Assessment of the seismic performance of two pile-deck wharf connections", *ASCE J. Perform. Constr. Facil.*, **25**(2), 98-104.

Blandon, C.A., Restrepo, J.I., Kawamata, Y. and Ashford, S. (2013), "Seismic performance of pile-supported wharves?", *Spec. Publ.*, **295**, 1-16.

Caiza-Sánchez, P. andrawes, B. and Lafave, J. (2012), "Analytical modeling and damage assessment of shallow embedment pile-deck connections", *Adv. Struct. Eng.*, **15**(10), 1673-1687.

Chiaramonte, M.M., Arduino, P., Lehman, D.E. and Roeder, C.W. (2013), "Seismic analyses of conventional and improved marginal wharves", *Earthq. Eng. Struct. Dyn.*, **42**(10), 1435-1450.

Doran, B., Shen, J. and Akbas, B. (2015), "Seismic evaluation of existing wharf structures subjected to earthquake excitation: case study", *Earthq. Spectra*, **31**(2), 1177-1194.

Erdogan, H., Doran, B., Seckin, A., Akbas, B., Celikoglu, Y. and Bostan, T. (2017), "Seismic performance and retrofit evaluation of an existing pile-wharf structure", *J. Perform. Constr. Facil.*, **31**(6), 04017110.

Giberson, M. (1967) "The response of nonlinear multistory structures subjected to earthquake excitations", Earthquake Engineering Research Laboratory, Pasadena.

Goel, R.K. (2010), "Approximate seismic displacement capacity of piles in marine oil terminals", *Earthq. Struct.*, **1**(1), 129-146.

Hines, E.M., Restrepo, J.I. and Seible, F. (2004), "Force-displacement characterization of well confined bridge piers", *ACI Struct. J.*, **101**(4), 537-548.

Johnson, G., Harn, R., Lai, C. and Jaradat, O. (2013) "The new ASCE standard for seismic design of piers and wharves", *Ports 2013: Success through Diversification*, 1345-1354.

Kawamata, Y., Blandon, C.A., Ashford, S. and Restrepo, J.I. (2007), "Seismic performance of container wharf piles for the port of Los Angeles", Test Report, Report No. TR 2007/06, Department of Structural Engineering, University of California, San Diego.

Larosche, A., Cukrov, M., Sanders, D. and Ziehl, P. (2014), "Prestressed pile to bent cap connections: Seismic performance of a full-scale three-pile specimen", *J. Bridge Eng.*, **19**(3), 04013012.

Lehman, D.E., Roeder, C., Stringer, S.J. and Jellin, A. (2013), "Seismic performance of improved pile-to-wharf deck connections", *PCI J.*, **53**(3), 62-80.

Mander, J.B., Priestley, M.J.N. and Park, R. (1984) "Seismic design of bridge piers", Research Report 84-2, Department of Civil Engineering, University of Canterbury, New Zealand.

Paulay, T. and Priestley, M.J.N. (1992) *Seismic Design of Reinforced Concrete and Masonry Buildings*, John Wiley and Sons, Inc.

PIANC (2002), Seismic Design Guidelines for Port Structures, A.A. Balkema Publishers.

Port of Long Beach (2012), Port of Long Beach Wharf Design Criteria, POLB WDC, Version 3.0.

Port of Los Angeles (2010), The Port of Los Angeles Seismic Code, The Port of Los Angeles.

Priestley, M.J.N. and Park, R. (1987), "Strength and ductility of concrete bridge columns under seismic loading", *ACI Struct. J.*, **84**(1), 61-76.

Priestley, M.J.N., Seible, F. and Calvi, G.M. (1996), *Seismic Design and Retrofit of Bridges*, John Wiley and Sons, Inc.

Restrepo, J.I., Park, R. and Buchanan, A.H. (1995), "Tests on connections of earthquake resisting precast reinforced concrete perimeter frames of buildings", *PCI J.*, **40**(4), 44-61.

Roeder, C.W., Graff, R., Soderstrom, J.L. and Yoo, J.H. (2001), "Seismic performance of pile-wharf connections", PEER Report 2002/07, Berkeley, California, December.

Shafieezadeh, A., DesRoches, R., Rix, G.J. and Werner, S.D. (2012), "Seismic performance of pile-supported wharf structures considering soil-structure interaction in liquefied soil", *Earthq. Spectra*, **28**(2), 729-757.

Sritharan, S. and Priestley, M.J.N. (1998), "Seismic testing of a full-scale pile-deck connection utilizing headed reinforcement", Report No. TR-98/14, La Jolla, California, August.

Srithartan, S. and Priestley, M.J.N. (1998), "Seismic testing of a full-scale pile-deck connection utilizing headed reinforcement", Report No. TR-98/14, La Jolla, California.

Su, L., Lu, J., Elgamal, A. and Arulmoli, A.K. (2017), "Seismic performance of a pile-supported wharf: Three-dimensional finite element simulation", *Soil Dyn. Earthq. Eng.*, **95**, 167-179.

Wang, T., Yang, Z., Zhao, H. and Wang, W. (2014), "Seismic performance of prestressed high strength concrete pile to pile cap connections", *Adv. Struct. Eng.*, **17**(9), 1329-1342.

Yang, Z. and Wang, W. (2016), "Experimental and numerical investigation on the behaviour of prestressed high strength concrete pile-to-pile cap connections", *KSCE J. Civil Eng.*, **20**(5), 1903-1912.

Zhao, J. and Sritharan, S. (2007), "Modeling of strain penetration effects in fiber-based analysis of reinforced concrete structures", *ACI Struct. J.*, **104**(2), 133-141.

CC

Notation

A_b = dowel bar cross section area
A_{sh} =Transverse reinforcement cross section area
d_b = reinforcing steel bar diameter
f'_c =concrete cylinder unconfined compressive strength for the pile or deck
f'_{cc} = confined concrete compressive strength

f_y	= yield strength of longitudinal reinforcement
f_{yh}	= yield stress of transverse reinforcement
H_n	= lateral force corresponding to the development of the pile nominal flexural strength, M_n
K_s	= experimental initial stiffness from the force controlled stage defined at cycles to 0.75 H_n
k	=unit transformation constant for estimation of plastic hinge length
L_p	= plastic hinge portion associated to regions above and below critical section where dowel bars are attached
δ_v	=deck vertical displacement
Δ	=applied lateral displacement
Δ_y	= yield displacement
ε_s	= strain in dowel reinforcement
ε_{smax}	=tensile strain at gage failure
ε_{smc}	= strain at peak stress of confining reinforcement
ε_{smd}	= strain at peak stress of dowel reinforcement
$\theta\varepsilon_{s1\%}$	=rotation at 1% tensile strain at dowel bar
$\theta\varepsilon_{smax}$	=rotation at ε_{smax}
μ_Δ	= displacement ductility
Θ	= connection drift ratio
θ	= connection rotation
ϕ	= connection section curvature
s	= transverse hoops spacing

Appendix I. Pile-deck joint principal tensile stress calculations

a. LS test specimen

The maximum joint shear force in test specimen LS can be determined from force equilibrium (Fig. A-1) and the compressive and tensile resultant forces at the pile deck interface (Fig. A-2) as follows:

Let:

v_j	= Joint shear stress
b_j	= Effective joint width
C_p^o	= Compressive force in connection at development of the plastic hinge
D	= Pile diameter
h_d	= Deck depth
l_{di}	= Distance between consecutive inflection points in the deck
l_{bi}	= Distance between tensile centroid at pile-deck connection and vertical component of hydraulic actuator force.
l_{pip}	= Distance to pile inflection point measured from the deck centerline
M_p^o	= Connection moment at development of the plastic hinge
P_c	= Axial compressive force
p_c	= Principal compressive stress
P_t	= Principal tensile stress
R_v^o	= Vertical component of hydraulic actuator force
R_h^o	= Horizontal component of hydraulic actuator force
T_p^o	= Tensile force in connection at development of the plastic hinge
V_{jh}	= Joint shear force
V_p^o	= Pile lateral force at the development of the plastic hinge

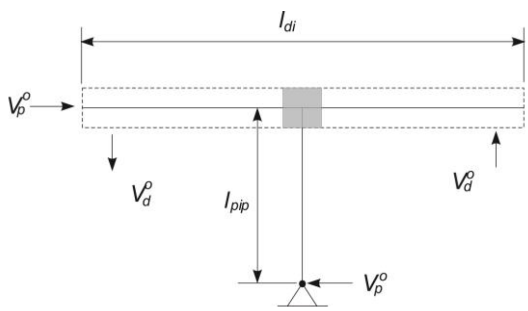

Fig. A-1 Joint shear force equilibrium

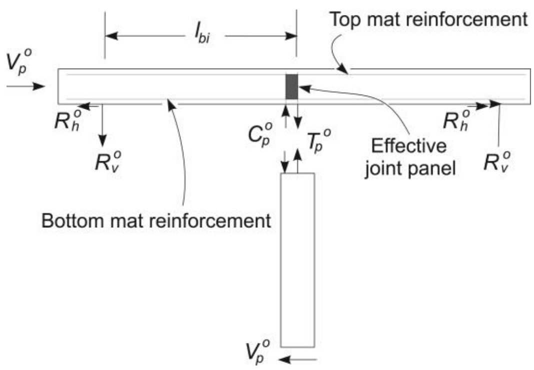

Fig. A-2 Free body diagram for connection LS

The joint shear stress corresponding to the joint shear force V_{jh} can be found as follows:

$$R_v^o = \frac{M_p^o}{2l_{bi}} = \frac{394\ kN - m}{5.8\ m} = 68\ kN$$

$$V_{jh} = R_v^o - T_p^o = 68\ kN - 1235\ kN$$

$$\upsilon_j = \left(\frac{V_{jh}}{Db_j}\right) = \left(\frac{1167\ kN}{610\ mm\ x\ 864\ mm}\right) = 2.2\text{MPa}$$

The accepted joint principal stresses corresponding to the joint shear force V_{jh} is defined according to Priestley *et al*. (1996):

$$f_h = \left(\frac{V_p^o}{b_jD}\right) = \left(\frac{191\ kN}{864\ mm\ x\ 610\ mm}\right) = 0.36MPa$$

$$p_{c/t} = \left(\frac{f_v + f_h}{2}\right) \pm \sqrt{\left(\frac{f_v - f_h}{2}\right)^2 + \upsilon_j^2}$$

$$p_c = 0.36 + \sqrt{0.36^2 + 2.2^2} = 2.6\ MPa$$

$$p_t = 0.36 - \sqrt{0.36^2 + 2.2^2} = -1.9\ MPa$$

The onset of joint cracking occurs when the principal tensile stress exceeds the tensile strength of concrete. Under combined loading, the tensile strength of concrete is very similar to the concrete uniaxial tensile strength. Therefore:

$$f_t = 0.29\sqrt{f_c'} = 2.1\ MPa$$

for the deck measured concrete compressive strength measured f'_c = 50 MPa

For the LS pile connection the ratio between the principal joint shear stress and the tensile strength of concrete is:

$$\frac{p_t}{f_t} = \frac{1.9\ MPa}{2.1\ MPa} = 0.89$$

b. HS test specimen

For the HS specimen the procedure is the same as for the LS connection, but due to the fluctuation of the axial load two values of the joint shear can be calculated. For the opening moment (pile in tension) the shear joint is as follows:

$$V_{jv} = C_p^o$$

$$C_p^o = T_p^o + R_p^o$$

$$T_p^o = 2570\ kN$$

$$C_p^o = V_{jv} = 2570\ kN - 681\ kN = 1889\ kN$$

$$\upsilon_j = \left(\frac{V_{jv}}{b_jh_d}\right) = \left(\frac{1889\ kN}{864\ mm\ x\ 864\ mm}\right) = 2.5\text{MPa}$$

The vertical component of the actuator force and the tensile force at the pile-deck connection are obtained from moment curvature iterative analyses and the geometry of the specimen. The same procedure can be followed for the closing moment (pile in compression) as given below. Note that in this case, the shear stress is obtained directly from the resultant tensile forces.

The same procedure can be followed for the closing moment (pile in compression) as given below. Note that in this case, the shear stress is obtained directly from the resultant tensile forces.

$$V_{jv} = T_p^o = 2570\ kN$$

$$\upsilon_j = \left(\frac{V_{jv}}{b_jh_d}\right) = \left(\frac{2570\ kN}{864\ mm\ x\ 864\ mm}\right) = 3.4\text{MPa}$$

The onset of joint cracking occurs when the principal shear stress exceeds the tensile strength of concrete as defined by Priestley *et al*. (1996):

$$f_t = 0.29\sqrt{f_c'} = 1.8\ MPa \quad \text{for f'}_c = 38\text{MPa}$$

The accepted joint principal stresses corresponding to the joint shear force V_{jh} is defined by Priestley *et al*. (1996) as:

$$f_v = \left(\frac{P_c}{b_j(D + 0.5h_d)}\right)$$

$$f_v = \left(\frac{680\ kN}{864\ mm(610\ mm + 0.5 * 864\ mm)}\right)$$

$$f_v = 0.7MPa$$

$$f_h = \left(\frac{V_p^o}{b_jD}\right) = \left(\frac{581\ kN}{864\ mm\ x\ 610\ mm}\right) = 1.1MPa$$

$$p_{c/t} = \left(\frac{f_v + f_h}{2}\right) \pm \sqrt{\left(\frac{f_v - f_h}{2}\right)^2 + \upsilon_j^2}$$

$$p_c = 0.09 + \sqrt{0.2^2 + 3.4^2} = 4.3\ MPa$$

$$p_t = 0.09 - \sqrt{0.2^2 + 3.4^2} = -2.5\ MPa$$

For the HS pile connection, and the most critical case (pile in compression), the ratio between the principal joint tensile stress and the tensile strength of concrete for the measured value of f'_c=38 MPa is:

$$\frac{p_t}{f_t} = \frac{2.5\ MPa}{1.8\ MPa} = 1.38$$